

Article

Determination of Mechanical Power Loss of the Output Mechanisms with Serially Arranged Rollers in Cycloidal Gears While Taking into Account Manufacturing Tolerances

Piotr Antoniak  and Sławomir Bednarczyk * 

Faculty of Mechanical Engineering, Wrocław University of Science and Technology, Wybrzeże Stanisława Wyspiańskiego 27, 50-370 Wrocław, Poland; piotr.antoniak@pwr.edu.pl

* Correspondence: slawomir.bednarczyk@pwr.edu.pl

Abstract: Despite their complex design, cycloidal gearboxes are characterized by high efficiency. Nevertheless, due to friction, some power is lost during gearbox operation. Basically, these losses occur in two structural nodes: the cycloid gearing and the output mechanism. Since the first of these nodes has been well discussed in the literature, the output mechanism will be discussed in this article. The design of the output mechanism has a significant impact on mechanical power losses. There are several mechanism design solutions. One of them is a mechanism with serially arranged rollers. Three solutions that are different in design but work identically will be discussed. Due to this affinity, a single, common mathematical model will be used to determine the value of losses. As will be shown, the value of losses is directly affected by the backlash, number, and diameter of the rollers used in the output mechanism and indirectly by the ratio and eccentricity of the cycloidal gearbox. Sample calculations were carried out using the developed model of mechanical power losses in the output mechanism. This made it possible to analyze the distribution of backlash created by manufacturing tolerances. It was also shown that the backlash has a significant effect on the number of rollers involved in torque transmission, as well as on the distribution of loads, contact pressures, and mechanical power losses.



Citation: Antoniak, P.; Bednarczyk, S. Determination of Mechanical Power Loss of the Output Mechanisms with Serially Arranged Rollers in Cycloidal Gears While Taking into Account Manufacturing Tolerances. *Machines* **2024**, *12*, 345. <https://doi.org/10.3390/machines12050345>

Academic Editor: Sheng Li

Received: 15 April 2024

Revised: 10 May 2024

Accepted: 13 May 2024

Published: 16 May 2024



Copyright: © 2024 by the authors. Licensee MDPI, Basel, Switzerland. This article is an open access article distributed under the terms and conditions of the Creative Commons Attribution (CC BY) license (<https://creativecommons.org/licenses/by/4.0/>).

Keywords: power losses; output mechanism; machining deviations; backlash; cycloidal gear

1. Introduction

Cycloidal gearboxes have several advantages, with high efficiency coming to the fore. This results from the fact that rolling nodes are used to transfer power from the input shaft to the output shaft, which includes the gearing, the output mechanism, and the central bearing node on the input shaft. In cycloidal reducers, the most commonly used output mechanism is one made of pins with bushings. The authors of [1] presented a method for determining the forces in the rolling nodes of a cycloidal reducer and determined its theoretical efficiency. In [2], a new concept of a cycloidal reducer is presented, for which a simplified method for determining the forces in the meshing is presented, and the theoretical mechanical efficiency based on experimental tests is described. In addition, the dependence of mechanical efficiency on speed and torque is also explained.

On the other hand, the authors of [3] presented and compared two methods (Malhotra's and Gorla's methods) for determining the efficiency of a single-stage cycloidal reducer. In [4], a comparative analysis of three analytical methods for determining the efficiency of a cycloidal drive is presented, and the results of the analyses are compared with the results of experimental tests. The effect of friction on the distribution of forces in the rolling nodes of the cycloidal reducer and the value of the friction torque and efficiency were discussed in [5]. In [6], the gearbox efficiency was determined using the reverse mechanism method. The authors of [7] presented an analysis of the effect of the mineral-based and synthetic lubricants used on the efficiency of a single-stage cycloidal gearbox based on experimental tests.

In [8], an analytical model of a cycloidal drive was developed, taking into account machining tolerances. It was noted that machining tolerances affect the backlash and the torque pulsation. Paper [9] presented an analysis of the performance of a cycloidal reducer with meshing machining tolerances using an approximate force distribution in a backlash-free cycloidal reducer. The authors of [10] presented an analytical method for determining losses in cycloidal gear meshing (epi- and hypocycloidal) considering the machining deviations of the meshing elements. Article [11] presents a method for the analysis of kinematic errors and the selection of machining tolerances in cycloidal reducers. For this purpose, the Monte Carlo method was used. A dynamic model for an accurate prediction of the number of rollers used to transfer the load in a cycloidal reducer with assembling backlash was presented in [12]; in this model, both normal and tangential forces were considered.

It is not only in the meshing that mechanical power losses occur that due to machining tolerances but also in the output mechanism. In [13], a model for the backlash and force distribution in the output mechanism of a cycloidal reducer, consisting of pins and bushings, was developed and analyzed with regard to machining deviations.

Cycloidal gearboxes are undergoing continuous development. One direction is the design of two-stage reducers [14,15], and even three-stage reducers [16]. In [14,15], the authors proposed two-stage reducers consisting of two cycloidal gears, one for each reduction stage. The differences lie in the way the drive is transferred from one stage to the other. In [14], a plate with pins was used, while the authors of [15] used a mechanism based on an Oldham clutch. A compact cycloidal gearbox, and, at the same time, a very high gear ratio were obtained by designing a three-stage reducer (virtual prototype) using an architecture called Nested [16]. It involves the use of epi- and hypocycloidal meshing, which eliminates the commonly used output mechanism in two stages. In this case, the meshing acts as an additional output mechanism.

The next stage of development is the use of different types of solutions for the output mechanism. Sometimes, it is a modification of an existing solution [17]. The ends of the pins were supported in rolling bearings, obtaining only rolling friction in the pin output mechanism. With this solution, the efficiency of the cycloid gearbox was improved. The authors of [18] proposed a novel method of optimizing the crankshaft bearings of Nabtesco RV reducer, in which rotational motion from the cycloidal gears is transmitted to the output disc using its stops, trapezoidal in shape, located in the trapezoidal holes of these gears. In [19], Nabtesco RV cycloidal reducer was compared with Spinea TwinSpin cycloidal reducer by determining the stresses and deformations of the reducers' main elements. The reducers differ from each other only if the output mechanism used. In the TwinSpin reducer, cross-shaped transformation elements are placed between the cycloidal gears and the output discs, whose motion is restricted by the stops of the cycloidal gears and rollers. The task of the transformation elements is to convert the planetary motion of the cycloidal gears into the rotary motion of the output discs.

The authors of the paper [20] compared two solutions of the cycloid gearbox, differing in the output mechanism. One gearbox was characterized by the output mechanism being a second-stage wheel rigidly connected to the output shaft (the Wolfrom configuration), while the other used the well-known pin output mechanism. This solution resulted in a smaller number of parts relative to the two-stage gearbox with a pin output mechanism. Publications [21,22] present a new solution of a single-stage cycloidal reducer with modified meshing and an output mechanism based on the cooperation of rollers with output disc stops. A new algorithm for determining the forces in the modified tooth profile was presented [21]. After analyzing the structure of the reducer, the places where the lost motion occurs were selected [22]. These are mainly the modified meshing and the output mechanism. Then, the lost motion in each of them, and finally, the whole reducer, was mathematically described. The theoretical analysis was verified experimentally. Alternatively, the author of [23] proposed adding an output mechanism made of a disc and four pins to a reducer with one or two cycloidal gears. An output mechanism composed of a

sliding plate and rollers cooperating simultaneously with the cycloidal gear and the output disc was presented in [9,24].

Cycloid gearboxes with a pin output mechanism are commonly used. They are widely described and studied [1–8,11–13]. Alternatively, mechanisms with rollers can be used. The output mechanisms presented in [9,19,21,22,24] can be classified as mechanisms with serially arranged rollers. The authors in these articles narrowly presented the output mechanisms, usually when analyzing the whole reducer.

In [9], the efficiency of a cycloid gearbox with backlash was determined by determining the power losses in the gearing, output mechanism, and bearing. Mathematical models of power losses were adopted for this purpose, including for the output mechanism. The FEM (Finite Elements Method) [9,24] was used to determine contact forces in the gearbox with backlash. This required building a numerical model of the gearbox based on the known geometry of its elements. In addition, the proposed model of power losses in the output mechanism is based on the assumption that there is sliding friction characterized by a constant friction coefficient. Another simplification that has been applied is that the motion (oscillation) of the rollers during the operation of the gearbox has been ignored. Power losses in the gearbox were estimated for the assumed clearance distributions; it was not indicated how they were determined. In turn, lost motion in the output mechanism was described in [22]. A mathematical expression has been derived in which the lost motion in the output mechanism is described as the angle by which the motion transforming element should rotate in order to cancel the backlash. Although some solutions have found their way into production using the TwinSpin reducer as an example [19], there are few studies on these output mechanisms. Knowing them in a broader context will make it possible to choose a solution in terms of mechanical losses.

This paper is an attempt to fill this gap by means of a developed mathematical model of power losses in a mechanism with serially arranged rollers of a universal nature. The mathematical model presented does not require the building of a numerical model. It was assumed that only rolling friction occurs in the mechanism. It was assumed that the rollers move in an oscillatory motion relative to the other elements of the mechanism. The influence of the geometry of the elements of the mechanism on the losses occurring in it was taken into account. Its form takes into account the machining deviations of the mechanism elements, which affect the backlash appearing in it and the uneven distribution of the load transferred by the rollers. For this purpose, a model was developed for the backlash distribution occurring in the mechanism, taking into account the machining deviations of its elements.

The contents of this article are organized as described below.

Section 2 describes the construction and principle of operation of an output mechanism with serially arranged rollers.

The determination of the backlash created by the manufacturing deviations of the components that make up the mechanism is presented in Section 3.

In Section 4, an expression describing the loads acting on the rollers, taking into account the backlash, is derived.

As a result of backlash in the mechanism, not all rollers are in contact with the other components. Hence, the effective number of rollers transferring torque was determined in Section 5.

Verification of the output mechanism with serially arranged rollers in terms of strength will be possible thanks to the contact stress model adopted in Section 6.

Section 7 presents a mathematical model of the mechanical loss of power in the output mechanism. Expressions describing backlash (Section 3), loads (Section 4), and the effective number of rollers (Section 5) were used to build it.

The results of the example calculations and their discussion are placed in Section 8.

Section 9 presents a summary and conclusions.

2. Design and Principle of Operation

The task of the output mechanism is to receive the movement from the cycloidal gears and transmit it to the output flange. When receiving motion, the planetary motion of the cycloidal gears is transformed into the rotational motion of the output flange. Figure 1 shows the structure of three different output mechanisms with rollers arranged in series. The main difference between them is the shape of the transformation member 4, which converts the planetary motion of the cycloidal gear 2 into the rotational motion of the output flange. In the solution from Figure 1a [19], it is a cross 4, while in Figure 1b [9,24], it is a cuboid-shaped sliding plate 4 with a square base. However, in the third solution, shown in Figure 1c [21,22], the transformation member 4 is a disc with cut-out holes. In addition to the transformation member 4, the output mechanism consists of sets of rollers 6 and 7, which cooperate with stops 5 of the cycloidal gear 2 and stops 8 of the output flange, respectively. Each set of rollers consists of n rollers. The shape of stops 5 and 8 often results from the shape of transformation member 4.

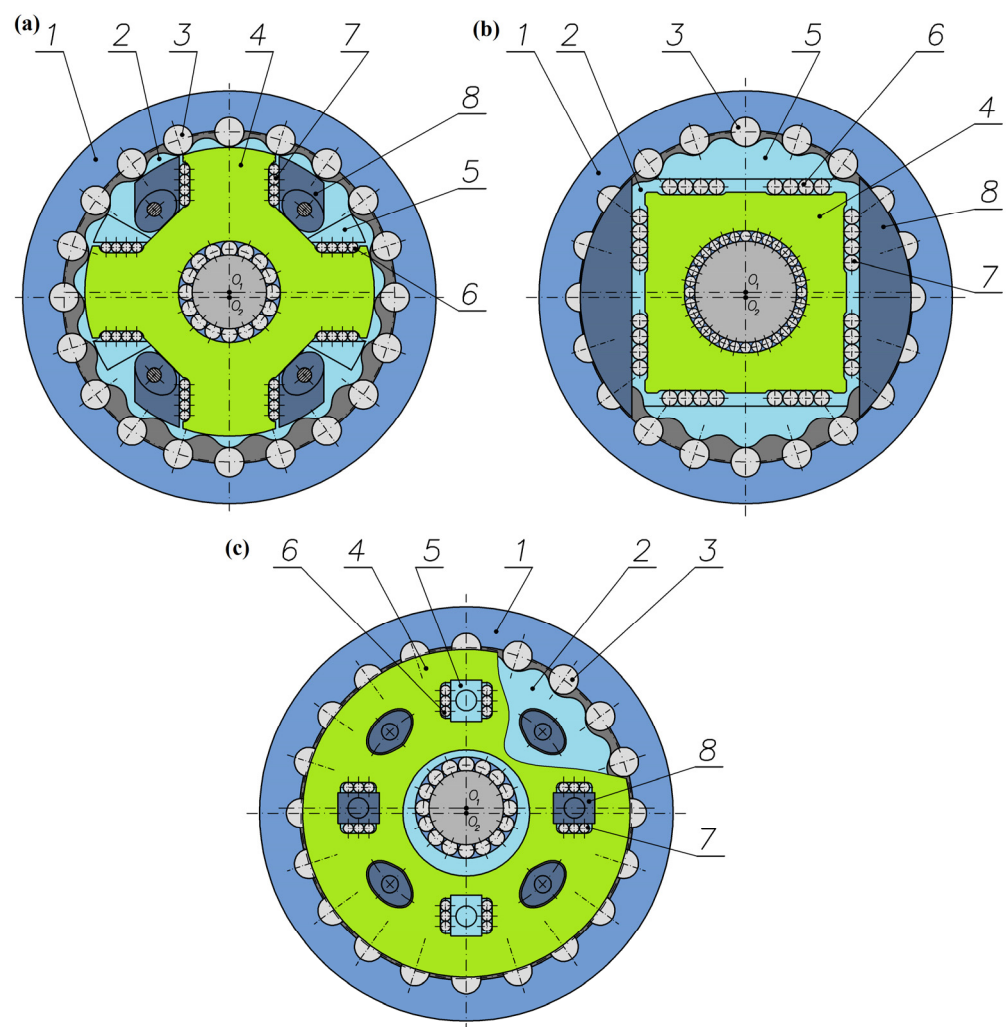


Figure 1. Structure of three different output mechanisms with rollers arranged in series: (a) a cross, (b) cuboid-shaped sliding plate with a square base and (c) disk with cut-out holes. 1—case; 2—cycloidal gear; 3—roller; 4—transformation member; 5—stop of cycloidal gear; 6, 7—set of rollers; 8—stop of output flange.

The principle of operation of the output mechanisms listed in Figure 1 is identical. When the cycloidal gear 2 rotates, the gear stops 5, via the rollers 6, exert pressure on the surfaces of the transformation member 4 parallel to the surfaces of the gear stops, thus causing the transformation member 4 to rotate. Then, the surfaces of the transformation

member 4, perpendicular to its surfaces and cooperating with the stops of the cycloidal gear 2, exert pressure through the rollers 7 on the output flange stops 8, causing the output flange to rotate.

In each solution presented in Figure 1, the transformation members 4 and stops 5 and 8 move relative to the roller sets 6 and 7, setting the rollers in rotary motion. Between them, there is an identical friction process, causing a loss of mechanical power regardless of the solution. The only difference between them is the distance of the sets of rollers from each other. In the solution (Figure 1b), set 6 is closest to set 7, while in the solution (Figure 1c), it is farthest. Nevertheless, this does not affect the fact that mechanical power losses occur differently.

Therefore, later in the paper, the determination of mechanical power losses in the output mechanism with rollers arranged in series will be discussed using the example of the solution in Figure 1b.

3. Backlash

The output mechanism of the cycloidal gearbox, as shown in Figure 2, consists of a sliding plate 4 and sets of rollers 6 and 7, which, respectively, cooperate with the stops of the cycloidal gear 2, taking torque M_K from the cycloidal gear 2. Then the rollers 7 acting on the stops 8 of the output flange transmit torque M_{sp} from the output mechanism to the output side of the cycloidal gearbox.

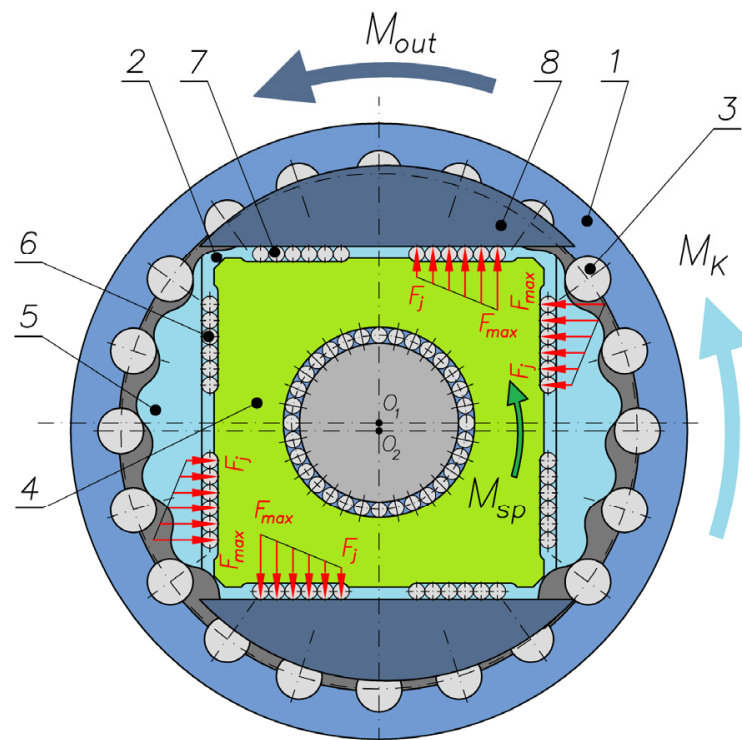


Figure 2. Output mechanism with a sliding plate (floating).

The components of the output mechanism are made with a certain tolerance, T . Thus, a backlash (initial) Δ appears between them. Figure 3 shows the machining tolerance of particular components that have an impact on the backlash Δ . The stops made in the cycloidal gear form a groove with a width b_k , while between the stops in the flange, there is a groove with a width b_t . Between the grooves is a sliding plate with side dimensions matching the dimensions b_k and b_t , respectively, and a roller with a diameter d_r . Thus, as a general solution, the base of the plate can be a rectangle.

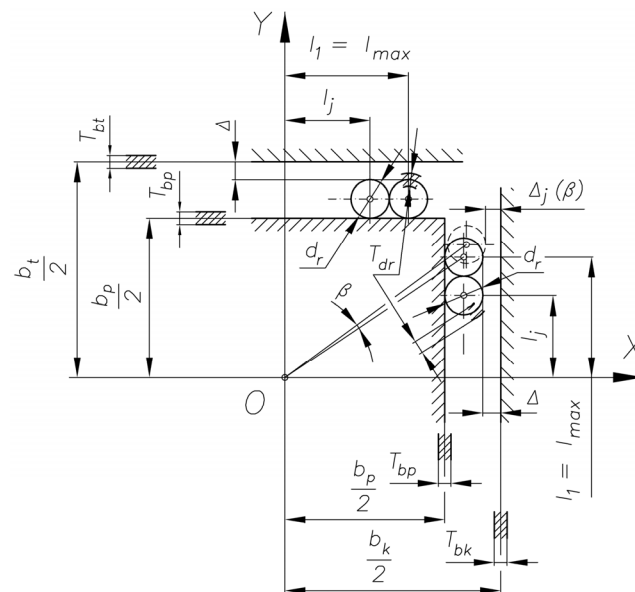


Figure 3. Machining tolerances.

Therefore, the following types of tolerance can be identified:

- Machining tolerance for the groove width b_k in the cycloidal gear— T_{bk} ;
- Machining tolerance for the width b_p of the sliding plate— T_{bp} ;
- Machining tolerance for the diameter d_r of the roller— T_{dr} ;
- Machining tolerance for the groove width b_t in the flange— T_{bt} .

The following assumptions were made to determine the backlash in the output mechanism Δ :

1. The machining tolerance T of the surfaces of the output mechanism components is distributed symmetrically as compared to the nominal dimension.
2. The surfaces of the output mechanism components cooperating with the rollers are parallel to each other.
3. All rollers in the output mechanism have identical machining deviations.
4. The meshing exerts no impact on the operation of the output mechanism.

As can be seen from the design of the output mechanism (Figure 3), backlash Δ occurs in two places between the following:

1. The sliding plate, rollers, and groove in the cycloid gear.
2. The sliding plate, rollers, and groove in the flange.

If the assumptions are met, backlash Δ takes a constant value.

Therefore, the backlash in the output mechanism between the sliding plate, the rollers, and the groove in the cycloidal gear can be determined as follows:

$$\Delta = \frac{(b_k + \delta_{bk}) - (b_p + \delta_{bp})}{2} - (d_r + \delta_{dr}) \quad (1)$$

Similarly, the backlash Δ between the sliding plate, rollers and groove in the flange is as follows:

$$\Delta = \frac{(b_t + \delta_{bt}) - (b_p + \delta_{bp})}{2} - (d_r + \delta_{dr}) \quad (2)$$

where

δ_{bk} —machining deviation of the groove width b_k in the cycloidal gear, within tolerance T_{bk} ;

δ_{bp} —deviation of the side of the sliding plate b_p in the cycloidal gear, within tolerance T_{bp} ;

δ_{dr} —machining deviation of the roller diameter d_r , within tolerance T_{dr} ;

δ_{bt} —machining deviation of the groove width b_t in the flange, within tolerance T_{bt} .

If the cycloidal gear is rotated by a very small angle β , then the backlash Δ between the grooves of the cycloidal gear, the rollers, and the sliding plate, will not be constant, and for the j -th roller, it will equal:

$$\Delta_j(\beta) = \Delta - \sin \beta \cdot l_j \quad (3)$$

where

l_j —the distance between the roller center and the OX or OY axis:

$$l_j = l_{\max} - (j - 1) \cdot d_r^* \quad (4)$$

where

d_r^* —the diameter of roller d_r with regard to the machining deviation δ_{dr} , $d_r^* = (d_r + \delta_{dr})$.

For very small angles β , it can be assumed that $\sin \beta = \beta$. Therefore, expression (3) takes the following form:

$$\Delta_j(\beta) = \Delta - \beta \cdot l_j \quad (5)$$

The same holds true for backlash Δ created between the stops of the flange, the rollers, and the sliding plate, with the difference that, in this case, the sliding plate rotates by angle β to the flange stops. For easier analysis and without making a mistake, it can be assumed that the sliding plate rotates by angle β to the stops of the cycloidal gear and the flange. Thus, in order to eliminate the backlash in the j -th roller, the sliding plate must be rotated by angle $\beta_{\Delta j}$, that is,

$$\beta_{\Delta j} = \frac{\Delta}{l_j} \quad (6)$$

It can be seen that rotating the sliding plate by angle $\beta_{\Delta j}$ removes the backlash Δ for the j -th roller and for all rollers with lower indices. In addition, the following conclusions follow from relation (6):

- Backlash Δ will be removed on the first roller after rotating the plate by an angle:

$$\beta_{\Delta 1} = \frac{\Delta}{l_1} = \frac{\Delta}{l_{\max}}$$

- Backlash Δ will be removed on the j -th roller after rotating the plate by angle:

$$\beta_{\Delta j} = \frac{\Delta}{l_j} = \frac{\Delta}{l_{\max} - (j - 1) \cdot d_r^*}$$

- Backlash Δ will be removed on the n -th (last) roller after rotating the plate by angle:

$$\beta_{\Delta n} = \frac{\Delta}{l_n} = \frac{\Delta}{l_{\max} - (n - 1) \cdot d_r^*}$$

- After rotating the plate by angle $\beta < \beta_{\Delta 1}$, no rollers will carry the load;
- After rotating the plate by angle $\beta < \beta_{\Delta j}$, only $j - 1$ rollers will carry the load;
- After rotating the plate by angle $\beta \geq \beta_{\Delta n}$, all rollers will carry the load.

4. Loads

As a result of the operation of the cycloidal gearbox, i.e., during the transmission of the torque M_K through the output mechanism, loads F_j , which are shown in Figure 2, occur. According to Hertz's theory [22], the value of the load F in the contact between the roller and the plane is equal to the following:

$$F = \frac{\pi}{4} \cdot E^* \cdot L \cdot \delta \quad (7)$$

where

$$\frac{1}{E^*} = \frac{1 - \nu_k^2}{E_k} + \frac{1 - \nu_r^2}{E_r} \text{ or } \frac{1}{E^*} = \frac{1 - \nu_p^2}{E_p} + \frac{1 - \nu_r^2}{E_r}, \text{ or } \frac{1}{E^*} = \frac{1 - \nu_t^2}{E_t} + \frac{1 - \nu_r^2}{E_r}$$

E_k —Young's modulus of the material of which the cycloidal gear is made;

E_r —Young's modulus of the material of which the roller is made;

E_p —Young's modulus of the material of which the sliding plate is made;

E_t —Young's modulus of the material of which the flange is made;

ν_k —Poisson's number of the material of which the cycloidal gear is made;

ν_r —Poisson's number of the material of which the roller is made;

ν_p —Poisson's number of the material of which the sliding plate is made;

ν_t —Poisson's number of the material of which the flange is made.

If the cycloidal gear, rollers, sliding plate, and flange are made of identical material, i.e., $E_k = E_r = E_p = E_t = E$ and $\nu_k = \nu_r = \nu_p = \nu_t = \nu$, the following can be written:

$$E^* = \frac{E}{2 \cdot (1 - \nu^2)}$$

L —the length of the roller;

δ —the displacement of the center of the roller under load F , causing deformation of the roller.

For the output mechanism under consideration, the displacement $\delta_j(\beta)$ of the centers of particular rollers can be represented as follows:

$$\delta_j(\beta) = \beta \cdot l_j - \Delta \quad (8)$$

In view of this, the load $F_j(\beta)$ occurring at the point of contact between the roller and the plane during cycloidal gearbox operation is as follows:

$$F_j(\beta) = \frac{\pi}{4} \cdot E^* \cdot L \cdot H_j \cdot \delta_j(\beta) = \frac{\pi}{4} \cdot E^* \cdot L \cdot H_j \cdot (\beta \cdot l_j - \Delta) \quad (9)$$

where

H_j —Heaviside function, defined as the following:

$$H_j = \begin{cases} 0, & \delta_j(\beta) < 0 \\ 1, & \delta_j(\beta) \geq 0 \end{cases} \quad (10)$$

The analysis of expression (9) shows that load $F_j(\beta)$ is proportional to the distance l_j . Considering expression (4) and the condition: $\delta_j(\beta) > 0$, i.e., when $H_j = 1$, the maximum load $F_{\max}(\beta)$ will occur at the contact of the 1st roller (Figure 2) and will equal the following:

$$F_{\max}(\beta) = F_1(\beta) = \frac{\pi}{4} \cdot E^* \cdot L \cdot (\beta \cdot l_{\max} - \Delta) \quad (11)$$

5. Effective Number of Rollers

During the operation of the cycloidal gearbox (Figure 2), torque M_K is transmitted during the interaction of the stops of the cycloidal gear with the rollers and the sliding plate and the interaction of the sliding plate with the rollers and the stops of the flange. Since there are two sets of n rollers in each assembly, the value of the total torque $M^n(\beta)$ transmitted by the rollers equals the following:

$$M^n(\beta) = 2 \cdot \sum_{j=1}^n M_j(\beta) \quad (12)$$

where

$M_j(\beta)$ —partial torque.

The partial torque $M_j(\beta)$ is generated by the load $F_j(\beta)$ acting on the arm l_j and can be calculated as follows:

$$M_j(\beta) = F_j(\beta) \cdot l_j \quad (13)$$

Substituting expression (8) into expression (13) yields the following:

$$M_j(\beta) = \frac{\pi}{2} \cdot E^* \cdot L \cdot H_j \cdot (\beta \cdot l_j^2 - \Delta \cdot l_j) \quad (14)$$

Therefore, the total torque $M^n(\beta)$ equals the following:

$$M^n(\beta) = \frac{\pi}{2} \cdot E^* \cdot L \cdot \sum_{j=1}^n H_j \cdot (\beta \cdot l_j^2 - \Delta \cdot l_j) = \frac{\pi}{2} \cdot E^* \cdot L \cdot \left[\beta \cdot \sum_{j=1}^n H_j \cdot l_j^2 - \Delta \cdot \sum_{j=1}^n H_j \cdot l_j \right] \quad (15)$$

During the operation of the cycloidal gearbox, the output mechanism transmits a torque equal to M_K , i.e., $M^n(\beta) = M_K$, which requires rotation of the mechanism by angle β_k . The value of angle β_k can be determined by transforming expression (15), which gives the following:

$$\beta_k = \frac{M_K + \frac{\pi}{2} \cdot E^* \cdot L \cdot \Delta \cdot \sum_{j=1}^n H_j \cdot l_j}{\frac{\pi}{2} \cdot E^* \cdot L \cdot \Delta \cdot \sum_{j=1}^n H_j \cdot l_j^2} = \frac{2 \cdot M_K}{\pi \cdot E^* \cdot L \cdot \sum_{j=1}^n H_j \cdot l_j^2} + \Delta \cdot \frac{\sum_{j=1}^n H_j \cdot l_j}{\sum_{j=1}^n H_j \cdot l_j^2} \quad (16)$$

However, as a result of the machining tolerances T adopted for the components of the output mechanism, backlash Δ , which occurs in it, takes on a value in the range $\Delta_{\min} \div \Delta_{\max}$. Consequently, a different number of rollers from the range $1 \div n$ may take part in the transmission of torque M_K , depending on the value of backlash Δ . It is, therefore, necessary to determine the effective number of rollers m from the range $1 \div n$ required to transfer the torque M_K for a given backlash Δ .

It is possible to determine the effective number of simultaneously cooperating rollers m required to transmit torque M_K by comparing the value of torque M_K with the value of the maximum torque M_{\max}^m . The value of torque M_{\max}^m is equal to the value of the total torque $M^n(\beta)$, calculated for a rotation of angle β , at which the backlash Δ for the $(m + 1)$ -th roller is removed (the transfer of a higher torque value required the use of the next, i.e., $(m + 1)$ -th roller). Thus, substituting the following into expression (15): $\beta = \beta_{\Delta(m+1)}$ and $n = m$, where $m < n$, we obtain the following:

$$M_{\max}^m = M^m(\beta_{\Delta(m+1)}) = \frac{\pi}{2} \cdot E^* \cdot L \cdot \sum_{j=1}^m (\beta_{\Delta(m+1)} \cdot l_j^2 - \Delta \cdot l_j) = \frac{\pi}{2} \cdot E^* \cdot L \cdot \left[\beta_{\Delta(m+1)} \cdot \sum_{j=1}^m l_j^2 - \Delta \cdot \sum_{j=1}^m l_j \right] \quad (17)$$

where:

$$\beta_{\Delta(m+1)} = \frac{\Delta}{l_{m+1}} = \frac{\Delta}{l_{\max} - m \cdot d_r^*} \quad (18)$$

It should be noted that under these assumptions (parallel walls, equal diameters of the rollers, etc.), the function H_j takes the value 1 for all m rollers. For the others (i.e., from $m + 1$ to n), the function H_j takes the value 0. For this reason, expression (15) is simplified to the form (17).

By substituting expression (18) into expression (17) and after transformations, one finally obtains the following:

$$M_{\max}^m = \frac{\pi \cdot E^* \cdot L \cdot \Delta \cdot d_r^*}{2 \cdot (l_{\max} - m \cdot d_r^*)} \cdot \sum_{j=1}^m (m - j + 1) \cdot l_j \quad (19)$$

By comparing the values of the maximum torques $M_{\max}^1, M_{\max}^2, \dots, M_{\max}^{n-2}, M_{\max}^{n-1}$ determined from expression (17) or (19) with the value of torque M_K , the effective number of rollers m is determined. The algorithm for determining the effective number of rollers m transferring torque M_K is shown in Figure 4. Knowing the number of rollers m necessary to

transmit torque M_K and using the expression (16), it is possible to determine the value of angle β_k^m , at which torque M_K is balanced by total torque $M^m(\beta)$:

$$\beta_k^m = \frac{2 \cdot M_K}{\pi \cdot E^* \cdot L \cdot \sum_{j=1}^m l_j^2} + \Delta \cdot \frac{\sum_{j=1}^m l_j}{\sum_{j=1}^m l_j^2} \quad (20)$$

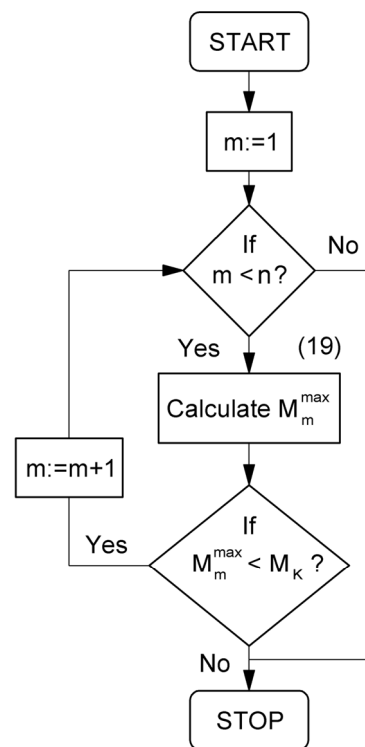


Figure 4. Algorithm for determining the effective number of rollers m .

By substituting $\beta = \beta_k^m$ into expression (11), we obtain the following:

$$F_{\max}^m = \frac{\pi}{4} \cdot E^* \cdot L \cdot (\beta_k^m \cdot l_{\max} - \Delta) \quad (21)$$

Similarly, substituting $\beta = \beta_k^m$ into expression (9), we obtain the following:

$$F_j^m = \frac{\pi}{4} \cdot E^* \cdot L \cdot (\beta_k^m \cdot l_j - \Delta) \quad (22)$$

6. Contact Stresses

At the contact points between rollers 5 and the side surfaces of plate 4, contact stresses $p_j(\beta)$ occur, as shown in Figure 2. Their distribution depends on the distribution of loads $F_j(\beta)$, and the pressures are shown as concentrated loads $F_j(\beta)$ at the contact points between the rollers 5.

The model shown in Figure 5 can be used to determine the contact stresses $p_j(\beta)$ [25,26].

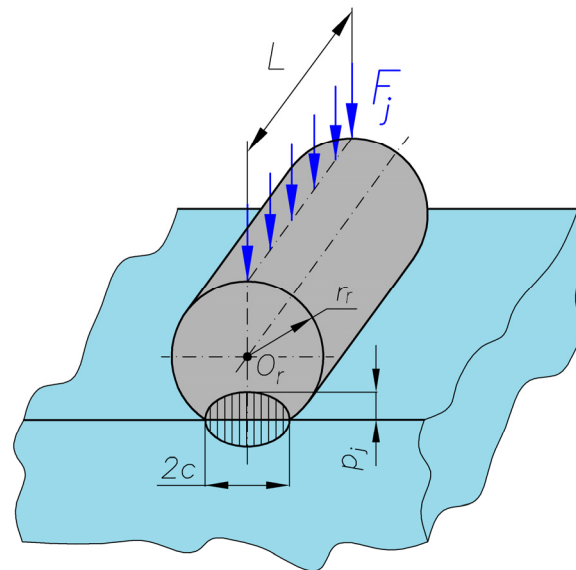


Figure 5. Contact stresses p_j [25,26].

The contact stresses p_j for the model in Figure 5 equal [25,26]:

$$p_j = \frac{2 \cdot F_j(\beta)}{\pi \cdot c \cdot L} \tag{23}$$

where

c —half of the contact width of the roller with the stop of the cycloidal gear, sliding plate or flange.

However, half of the contact width between the roller and the cycloidal gear stop c is determined from expression (24) [25,26]:

$$c = \sqrt{\frac{2 \cdot F_j(\beta) \cdot d_r^*}{\pi \cdot L \cdot E^*}} \tag{24}$$

7. Mechanical Power Losses

A cycloidal gearbox is characterized by the fact that the center of the cycloidal gear O_1 is displaced by an eccentricity e relative to the center of rotation O_2 of the input shaft. The rotating input shaft with center O_2 rotates the eccentric bearing, thus forcing the cycloidal gear to roll along the circumference of the stationary central gear with rollers (Figure 6).

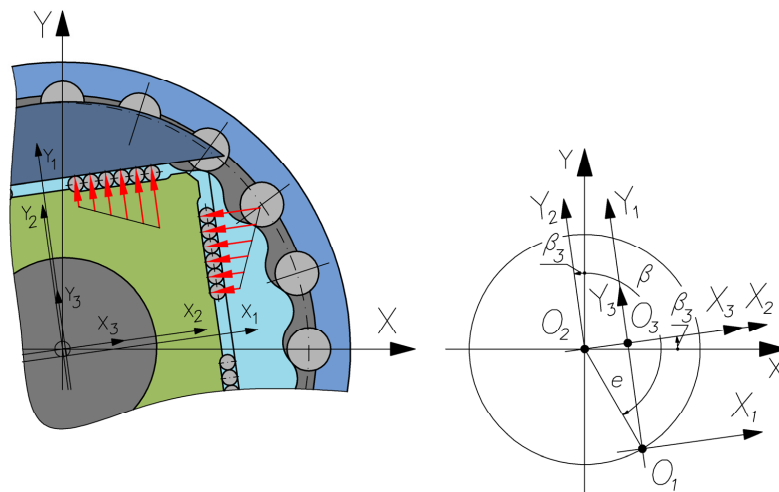


Figure 6. Operating principle of the output mechanism.

During gearbox operation, the cycloidal gear rolls to one side inside the central gear with rollers and simultaneously rotates in the opposite direction around its own axis. The meshing of the teeth of the cycloidal gear with the rollers of the central gear causes the rotation around its own axis. This cooperation causes center O_1 of the cycloidal gear to move along a circle with a radius equal to eccentricity e relative to the center of rotation O_2 of the input shaft. The rotational motion of the cycloidal gear is transmitted to the output shaft, of which the flange is an integral part, by means of a sliding plate placed between the stops of the cycloidal gear and the flange. It should be noted that during the operation of the mechanism, the position of the center of the flange is fixed and corresponds with the center of rotation O_2 of the input shaft. It is, however, quite different with the center of rotation O_3 of the sliding plate, which constantly changes its position, thus determining a rather complicated motion path, examples of which are shown in Figure 7. In turn, expression (25) describes the coordinates of the position of center O_3 depending on the rotation angle β of the input shaft. As can be seen, the motion path of center O_3 depends on the transmission ratio u of the cycloidal gearbox and eccentricity e . The number of branches of the motion path corresponds to the value $u + 1$, and they span within a circle of radius equal to e .

$$\begin{aligned} O_{3x} &= e \cdot \sin\left(\frac{u+1}{1} \cdot \beta\right) \cdot \cos\left(\frac{\beta}{u}\right) \\ O_{3y} &= e \cdot \sin\left(\frac{u+1}{1} \cdot \beta\right) \cdot \sin\left(\frac{\beta}{u}\right) \end{aligned} \quad (25)$$

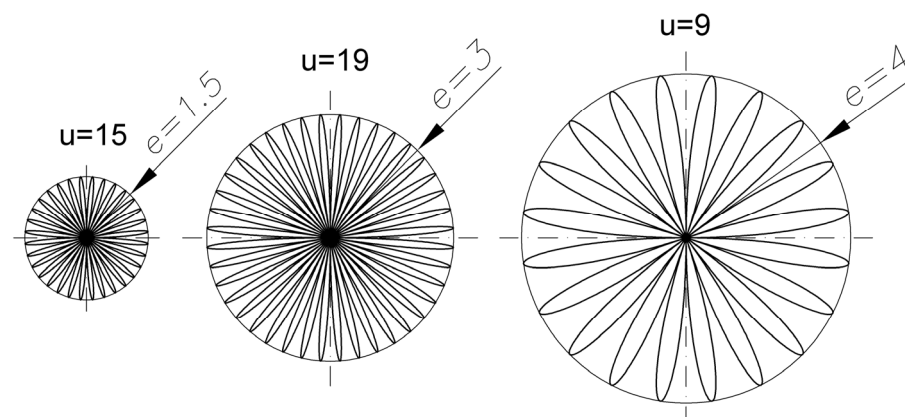


Figure 7. Motion path of the rotation center of the sliding plate.

Rollers are placed between the side surfaces of the sliding plate and the side surfaces of the stops of the cycloidal gear and flange. During the operation of the output mechanism, the angular velocities of the cycloidal gear ω_k , the sliding plate ω_p , and the flange ω_t are equal. However, it should be noted that this does not mean that there is no relative motion of the mentioned components. On the contrary, by analyzing the interaction between the cycloidal gear and the sliding plate, it can be shown that the center of the sliding plate O_3 moves relative to the center of the cycloidal gear O_1 in the direction of axis Y_1 . At the same time, the center of the sliding plate O_3 moves relative to the center of the flange O_2 in the direction of axis X_2 . The motion of the cooperating surfaces of the stops of the cycloidal gear with the surfaces of the sliding plate takes place with a relative linear velocity of v_{k-p} .

Similarly, the motion of the cooperating surfaces of the sliding plate with the flange stops takes place with a relative linear velocity of v_{p-t} . Since there are rollers between these surfaces, they are put into rotational motion with angular velocities ω_{k-p} and ω_{p-t} , respectively. This process is illustrated in Figure 8. Thus, there is friction between these components, causing a mechanical loss of power P_C in the output mechanism. There are four sets of n rollers in the mechanism: two sets related to the cooperation of the rollers with the side surfaces of the cycloidal gear and the sliding plate, and another two related to the cooperation of the rollers with the side surfaces of the sliding plate and the flange.

Considering the backlash, torque M_K is transmitted by the effective number of rollers m in each set.

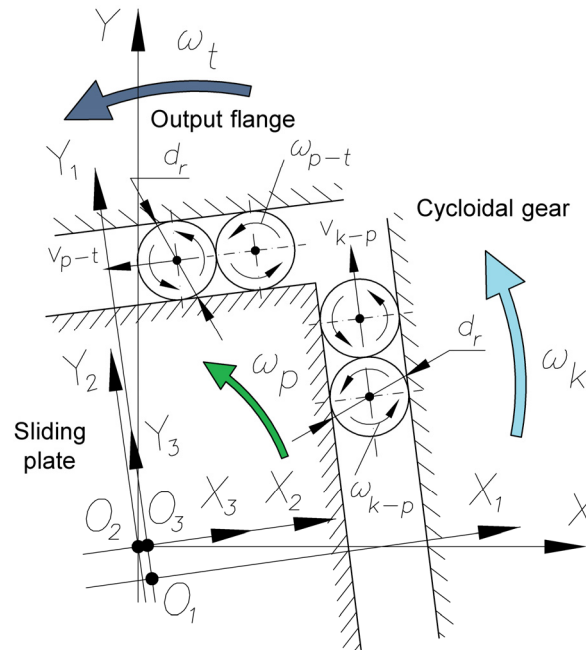


Figure 8. Angular velocities of the elements of the output mechanism.

Therefore, the total mechanical power loss P_C in the output mechanism of a cycloidal gearbox is the sum of the losses due to friction of the rollers against the surfaces of the cycloidal gear and the sliding plate, and friction of the rollers against the surfaces of the sliding plate and the flange, i.e.,

$$P_C = P_{k-p} + P_{p-t} \tag{26}$$

Loss of mechanical power in the output mechanism due to friction of the rollers against the surfaces of the cycloidal gear and the sliding plate equals:

$$P_{k-p} = \sum_{j=1}^m F_j(\beta) \cdot f_{r-k} \cdot |\omega_{k-p}(\beta)| + \sum_{j=1}^m F_j(\beta) \cdot f_{r-p} \cdot |\omega_{k-p}(\beta)| \tag{27}$$

where

- f_{r-k} —rolling friction coefficient between the rollers and the cycloidal gear;
- f_{r-p} —rolling friction coefficient between the rollers and the sliding plate;
- ω_{k-p} —angular velocity of the roller placed between the cycloidal gear and the sliding plate.

If the rollers, the cycloidal gear, and the sliding plate are made of the same material, it can be expressed as follows:

$$f_{r-k} = f_{r-p} = f \tag{28}$$

For the adopted model (Figure 5), i.e., the cooperation of a roller with a flat surface, the rolling friction coefficient f between the rollers and the sliding plate can be determined by expression (29) [27]:

$$f = \frac{\mu}{2} \cdot c \tag{29}$$

where

- μ —coefficient of sliding friction;
- c —half of the contact width of the roller with the gear stop, as defined by expression (24).

After substituting expression (28) into expression (27) and after transformations, taking into account that in the initial mechanism, the cycloidal gear, and the sliding plate together with the rollers cooperate in two places, the following result is obtained:

$$P_{k-p} = 4 \cdot f \cdot \left| \omega_{k-p}(\beta) \right| \sum_{j=1}^m F_j(\beta) \quad (30)$$

Similarly, there is a loss of mechanical power in the output mechanism due to friction of the rollers against the surfaces of the sliding plate and the flange:

$$P_{p-t} = \sum_{j=1}^m F_j(\beta) \cdot f_{r-k} \cdot \left| \omega_{p-t}(\beta) \right| + \sum_{j=1}^m F_j(\beta) \cdot f_{r-t} \cdot \left| \omega_{p-t}(\beta) \right| \quad (31)$$

where

f_{r-t} —coefficient of rolling friction between the rollers and the flange;

ω_{p-t} —angular velocity of the roller placed between the sliding plate and the flange.

Proceeding in a similar way to the loss of mechanical power in the output mechanism due to the friction of the rollers against the surfaces of the cycloidal gear and the sliding plate, the final result is obtained:

$$P_{p-t} = 4 \cdot f \cdot \left| \omega_{p-t}(\beta) \right| \sum_{j=1}^m F_j(\beta) \quad (32)$$

After substituting expressions (30) and (32) into expression (27), we obtain the following:

$$P_C = 4 \cdot f \cdot \left[\left| \omega_{k-p}(\beta) \right| + \left| \omega_{p-t}(\beta) \right| \right] \sum_{j=1}^m F_j(\beta) \quad (33)$$

As can be seen, the angular velocity of each roller of the output mechanism is a function of the position of the input roller β of the gear shown in Figure 6.

The angular velocities of the rollers can be determined from expressions (34) and (36):

- For the roller placed between the cycloidal gear and the sliding plate,

$$\omega_{k-p}(\beta) = \frac{v_{k-p}(\beta)}{d_r^*} = -\frac{u+1}{u} \cdot \frac{e}{d_r^*} \cdot \omega_0 \cdot \sin\left(\frac{u+1}{u} \cdot \beta\right) \quad (34)$$

where

$v_{k-p}(\beta)$ —linear speed of the roller placed between the cycloidal gear and the sliding plate.

Using Figure 6 and expression (25), the linear velocity of the roller placed between the cycloidal gear and the sliding plate $v_{k-p}(\beta)$ can be determined as follows:

$$v_{k-p}(\beta) = \frac{d}{dt}(O_{1y} - O_{3y}) = -e \cdot \frac{u+1}{u} \cdot \sin\left(\frac{u+1}{u} \cdot \beta\right) \cdot \frac{d\beta}{dt} \quad (35)$$

- For the roller placed between the sliding plate and the flange,

$$\omega_{p-t}(\beta) = \frac{v_{p-t}(\beta)}{d_r^*} = +\frac{u+1}{u} \cdot \frac{e}{d_r^*} \cdot \omega_0 \cdot \cos\left(\frac{u+1}{u} \cdot \beta\right) \quad (36)$$

where

$v_{p-t}(\beta)$ —linear speed of the roller placed between the sliding plate and the flange.

Similarly to the determination of the velocity $v_{k-p}(\beta)$, the linear velocity of the roller placed between the sliding plate and the flange $v_{p-t}(\beta)$ can be determined as follows:

$$v_{p-t}(\beta) = \frac{d}{dt}(O_{3x} - O_{2x}) = +e \cdot \frac{u+1}{u} \cdot \cos\left(\frac{u+1}{u} \cdot \beta\right) \cdot \frac{d\beta}{dt} \quad (37)$$

Substituting expressions (34) and (36) into expression (33), after necessary transformations one obtains the following:

$$P_C = \frac{4 \cdot e \cdot f \cdot \omega_0 \cdot (u + 1)}{u \cdot d_r^*} \cdot \left[\left| \cos\left(\frac{u + 1}{u} \cdot \beta\right) \right| + \left| \sin\left(\frac{u + 1}{u} \cdot \beta\right) \right| \right] \sum_{j=1}^m F_j(\beta) \quad (38)$$

The sum of the trigonometric functions from expression (36) is a periodic function, as shown in Figure 9. It can be seen that the period of the sum of trigonometric functions equals $\frac{1}{4}$ of the period T of its component functions and is determined from expressions (39) and (40):

$$\frac{u + 1}{u} \cdot \omega_0 \cdot T = 2 \cdot \pi \rightarrow T = \frac{2 \cdot \pi \cdot u}{(u + 1) \cdot \omega_0} \quad (39)$$

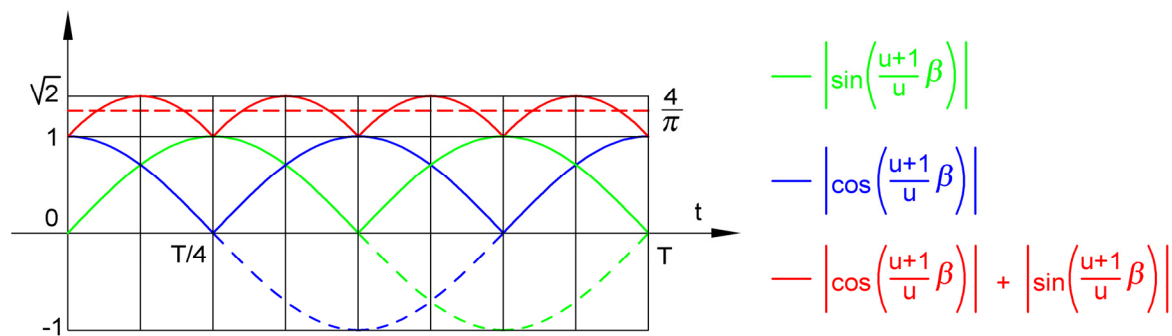


Figure 9. Graph of the sum of the trigonometric functions.

Thus,

$$\frac{T}{4} = \frac{\pi \cdot u}{2 \cdot (u + 1) \cdot \omega_0} \quad (40)$$

From the graph shown in Figure 9, the sum of the periodic function can be estimated as follows:

$$1 \leq \left| \cos\left(\frac{u + 1}{u} \cdot \omega_0 \cdot T\right) \right| + \left| \sin\left(\frac{u + 1}{u} \cdot \omega_0 \cdot T\right) \right| \leq \sqrt{2} \quad (41)$$

The mean value of the periodic function can also be determined from the following equation:

$$\frac{\int_0^{\frac{T}{4}} \left[\left| \cos\left(\frac{u + 1}{u} \cdot \beta\right) \right| + \left| \sin\left(\frac{u + 1}{u} \cdot \beta\right) \right| \right] dt}{\frac{T}{4}} = \frac{\int_0^{\frac{T}{4}} \left[\cos\left(\frac{u + 1}{u} \cdot \beta\right) + \sin\left(\frac{u + 1}{u} \cdot \beta\right) \right] dt}{\frac{T}{4}} = \frac{4}{\pi} \quad (42)$$

By substituting the final result of expression (40) into expression (36), we obtain an expression describing an average value of the power loss P_C in the following output mechanism:

$$P_C = \frac{4 \cdot e \cdot f \cdot \omega_0 \cdot (u + 1)}{u \cdot d_r^*} \cdot \frac{4}{\pi} \cdot \sum_{j=1}^m F_j(\beta) = \frac{16 \cdot e \cdot f \cdot \omega_0 \cdot (u + 1)}{\pi \cdot u \cdot d_r^*} \cdot \sum_{j=1}^m F_j(\beta) \quad (43)$$

8. Calculation Example

To verify the developed mathematical model of mechanical power loss in the output mechanism of Figure 2 and analyze it, two cases of the mechanism in question were considered. The cases considered differ mainly in the number of rollers n and diameter d_r . They were used in cycloidal gearboxes with the same ratio u and eccentricity e , as shown in Figure 10. In case 1, eight sets with $n = 6$ rollers with a diameter $d_r = 6$ [mm] were used, while in case 2, $n = 4$ rollers with diameter $d_r = 9$ [mm] were used in each set. The values of geometrical features, machining deviations, material properties, and load are summarized in Table 1. It can thus be seen that in both cases, identical values of groove width in the cycloidal gear b_k , groove width in the flange b_t , identical materials (E , ν), and machining deviations δ were adopted. The mechanisms differ in the values of the sides

of the sliding plate b_p due to the selection of rollers with different diameters d_r . For such causes, the mathematical model of the mechanical power losses in the output mechanism was analyzed in two stages. In stage one, a mechanism with no backlash was considered in order to determine the effect of the number and diameter of the rollers on the mechanical power loss. The second stage of the analysis considered the machining deviations of the elements that make up the output mechanism. This made it possible to determine the clearance between the rollers and the groove surfaces of the cycloid gear and the flange, and consequently its effect on mechanical power losses.

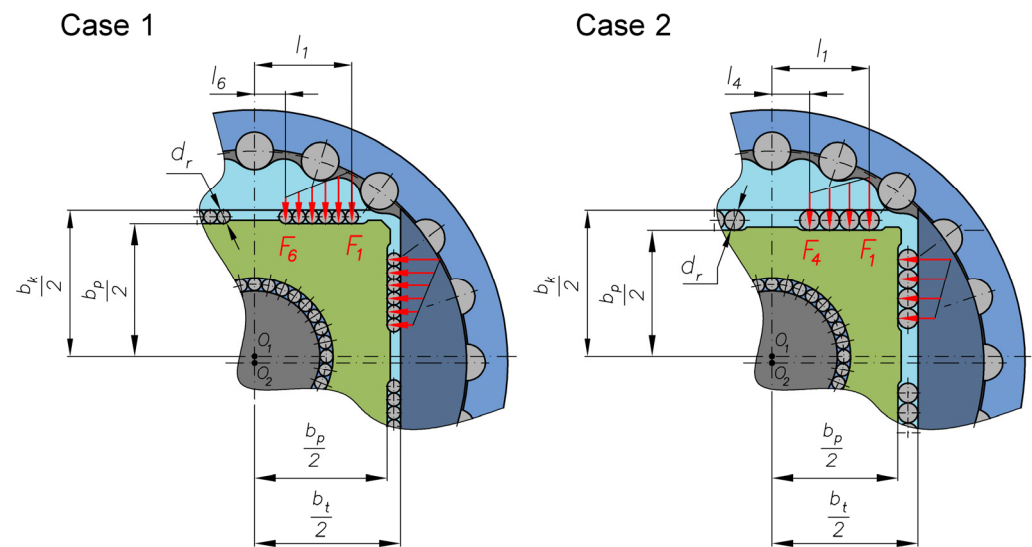


Figure 10. Geometrical features of the output mechanism.

Table 1. Summary of dimensions, material data, and machining deviations of the output mechanism components.

Name	Symbol	Unit	Value Case 1	Value Case 2
Number of rollers in the set	n	-	6	4
Roller diameter	d_r	[mm]	6	9
Roller length	L	[mm]		30
Distance from the first roller to the vertical axis of the gear	l_1	[mm]		44
Groove width in the cycloidal gear	b_k	[mm]	132	132
Groove width in the flange	b_t	[mm]	132	132
Sliding plate side	b_p	[mm]	120	114
Transmission ratio	u	-		19
Eccentricity	e	[mm]		3
Deviation of roller diameter	δ_{dr}	[mm]		0.005
Machining deviation of groove width in cycloidal gear	δ_{bk}	[mm]		0.025
Machining deviation of groove width in flange	δ_{bt}	[mm]		0.025
Machining deviation of the sliding plate side	δ_{bp}	[mm]		0.015
Young's modulus of the cycloidal gear, flange, sliding plate and rollers	E	[GPa]		207
Poisson's number of cycloidal gear, flange, sliding plate and rollers	ν	-		0.3
Load torque on the cycloidal gear	M_K	[Nm]		440

Realizing stage 1, the expression (20) was used to determine the angle β_k^m by which the sliding plate must rotate to balance the torque M_K . The loads $F_j(\beta)$ acting at the contact between the rollers and the side surface of the sliding plate were determined using equation (22). And the contact pressures $p_j(\beta)$ were determined using expressions (23) and (24). Finally, the mechanical power losses P_C were estimated using equation (43). In a backlash-free output mechanism, i.e., $\Delta = 0$ [mm], all the rollers in the set take part in the

transmission of load torque M_K , i.e., $m = n$. Thus, for case 1, the number of active rollers in the set is $m = 6$, and for the second case, $m = 4$. Figure 11 summarizes the calculations of loads $F_j(\beta)$, contact pressure $p_j(\beta)$, and mechanical power losses P_C for both cases of the backlash-free mechanism.

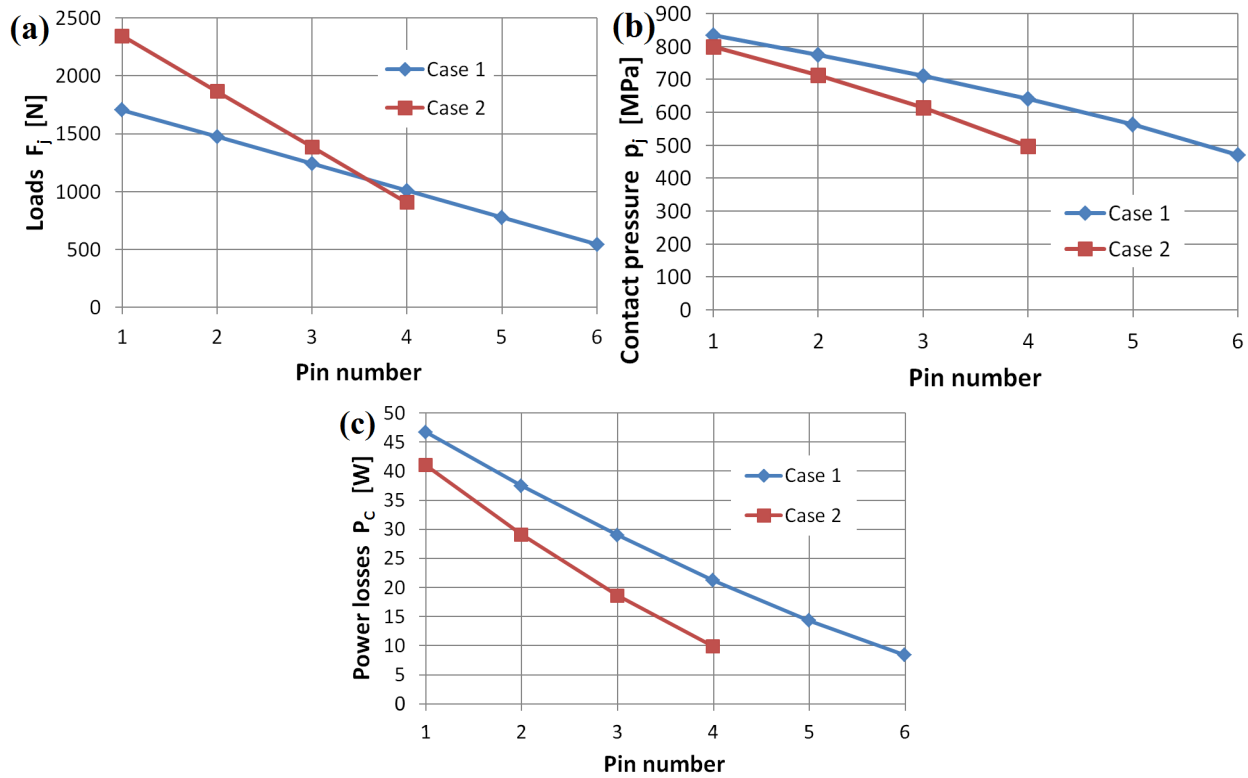


Figure 11. Calculation results of (a) loads, (b) contact pressure and (c) power losses for a backlash-free output mechanism.

Despite the higher values of loads $F_j(\beta)$ (Figure 11a) in the second case, in which $n = 4$ rollers with diameter $d_r = 9$ [mm] in each set were used, the contact pressure $p_j(\beta)$ (Figure 11b) and mechanical power losses P_C (Figure 11c) are smaller than in the first case, in which $n = 6$ rollers with diameter $d_r = 6$ [mm] were used.

This means that increasing the diameter d_r of the rollers, despite reducing the number of rollers n , which increases the value of loads $F_j(\beta)$, has a beneficial effect on reducing the value of power losses P_C . The value of the angle β_k^m by which the sliding plate must rotate to balance torque M_K and the sum of the mechanical losses P_C in the output mechanism are summarized in Table 2.

Table 2. Total mechanical losses for a backlash-free output mechanism.

Name	Symbol	Unit	Value Case 1	Value Case 2
Number of rollers in the set participating in the transmission of load torque M_K	m	-	6	4
The angle by which the sliding plate must rotate to balance torque M_K	β_k^m	[rad]	1.43×10^{-5}	1.96×10^{-5}
Total mechanical losses	P_C	[W]	157.14	98.65

Analyzing the results of the calculations of angle β_k^m and mechanical power losses P_C summarized in Table 2, it is noticeable that angle β_k^m takes on greater values for case 2.

In the second stage, the machining deviations of the groove width in the cycloidal gear δ_{bk} , the flange δ_{bt} , the side of the sliding plate δ_{bp} , and the roller diameter δ_{dr} were taken

into account in the calculations. Their values are presented in Table 1. Using expressions (1) or (2), the backlash was determined, which amounted to $\Delta = 0.005$ [mm] for all rollers in both cases. Based on expressions (3) and (4), the distribution of the backlash $\Delta_j(\beta)$ in the output mechanism was determined for both cases under consideration, as shown in Figure 12. The distribution of the backlash $\Delta_j(\beta)$ was obtained by rotating the cycloidal gear by angle β , enabling contact of the first roller of the mechanism with the surface, forming the groove in the cycloidal gear. Thus, on the first roller, the backlash Δ has been removed.

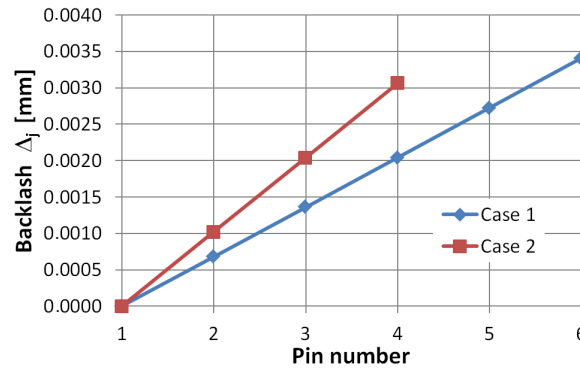


Figure 12. Distribution of backlash $\Delta_j(\beta)$ in the output mechanism.

As can be seen, the distribution of backlash $\Delta_j(\beta)$ for both cases is linear, but the values differ. In case 2, the values are larger than in case 1.

Proceeding as in the first stage, the distribution of forces $F_j(\beta)$ (22), the distribution of contact pressures $p_j(\beta)$ (23) and (24), and the distribution of mechanical power losses P_C (43) were determined, while the number of rollers m carrying the torque M_K and the angle β_k^m by which the sliding plate must rotate to balance the torque M_K were determined from the algorithm in Figure 4 and expressions (19) and (20). The results of the calculations are summarized in Figure 13.

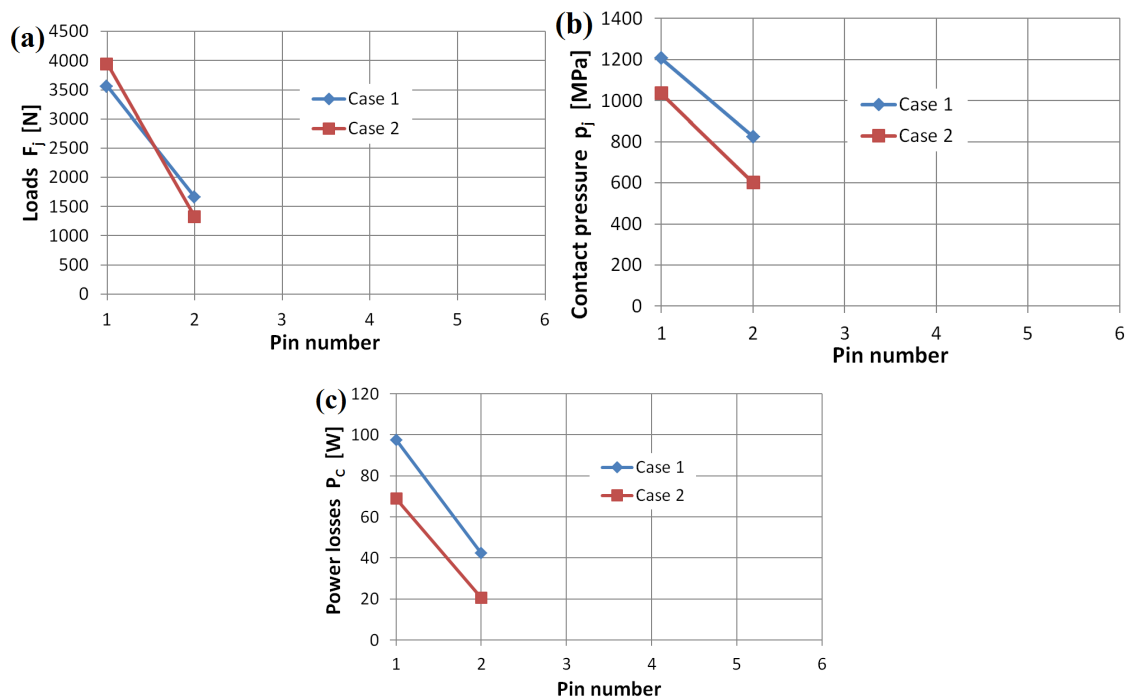


Figure 13. Calculation results of (a) loads, (b) contact pressure and (c) power losses for the output mechanism with backlash.

For the determined backlash $\Delta = 0.005$ [mm], resulting from the assumed deviations δ , and the distribution of the backlash $\Delta_j(\beta)$ resulting from the operation of the gear (Figure 12), it was observed that only two rollers take part in the transmission of load torque M_K , i.e., $m = 2$. The maximum value of load $F_j(\beta)$, appearing on the first roller, is higher in case 2 than in case 1, similar to the gear without backlash in the output mechanism. However, the value of contact pressure $p_j(\beta)$ is smaller at the contact point between the two rollers in the case with $n = 4$ rollers in each set than for the mechanism with $n = 6$ rollers. The situation is similar to the mechanical power losses P_C . They obtain smaller values in case 2 than in case 1. The reason for this is the diameter of the rollers d_r . A larger diameter d_r (case 2) causes smaller values of contact pressure $p_j(\beta)$ and mechanical power losses P_C . In contrast, the situation is different for the angle β_k^m , by which the sliding plate must rotate in order to balance torque M_K .

Its values and the sum of the mechanical power losses P_C are listed in Table 3. For the mechanism of case 2, this angle obtains greater values than in case 1, similar to mechanisms without backlash. On the other hand, in case 2, losses P_C take on smaller values, which results from the smaller value of the roller diameter d_r .

Table 3. Total mechanical losses for the output mechanism with backlash.

Name	Symbol	Unit	Value Case 1	Value Case 2
Number of rollers in the set participating in the transmission of load torque M_K	m	-	2	2
The angle by which the sliding plate must rotate to balance torque M_K	β_k^m	[rad]	14.52×10^{-5}	15.05×10^{-5}
Total mechanical losses	P_C	[W]	139.85	89.79

Comparing the calculations for gearboxes with output mechanisms without backlash (Figure 11) and with backlash (Figure 13), it can be seen that in the case of the mechanism with backlash, a smaller number of rollers m take part in the transmission of load torque M_K than in the gear with a mechanism without backlash; as a result, higher values of loads $F_j(\beta)$, contact pressure $p_j(\beta)$, and mechanical power losses P_C occur in the contact point between the rollers and the other elements forming the mechanism. In contrast, the total sum of the mechanical power losses P_C (Tables 2 and 3) is smaller in the mechanism with backlashes, but, in turn, the value of angle β_k^m by which the sliding plate must rotate in order to balance torque M_K is considerably larger. This results in less precision in the operation of the cycloidal gearbox using the mechanism with backlash, even though the mechanical power losses P_C are smaller.

9. Summary and Conclusions

Based on the construction, the principle of operation, and the geometrical dependencies of the output mechanism of a cycloidal gearbox consisting of a sliding plate cooperating with rollers, a mathematical model (43) of the mechanical power losses P_C was developed in the output mechanism with serially arranged rollers. In the discussed model, the machining deviations of the mechanism elements were considered. To this end, the distribution of backlashes $\Delta_j(\beta)$ was determined using expressions (3) and (4). Next, using expression (19) and the algorithm from Figure 4, the number of rollers m required to transfer the torque M_K and the distribution of loads $F_j(\beta)$ were determined using expression (23) and contact pressure $p_j(\beta)$, which is defined by expression (24). The graphical form of the distribution of backlash $\Delta_j(\beta)$, loads $F_j(\beta)$, contact pressure $p_j(\beta)$, and mechanical power losses P_C in the output mechanism without backlash and with backlash is presented in Figures 11–13, respectively, using the data summarized in Table 1. After analyzing the mathematical model of mechanical power losses P_C presented in the article and the obtained calculation results, the following conclusions can be drawn:

1. In terms of mechanical power losses P_C , it is advantageous to use fewer n rollers with a larger diameter d_r , as indicated by the distribution of losses P_C shown in Figures 11c and 13c. The sum of mechanical power losses P_C (Tables 2 and 3) is smaller for case 2. Comparisons were made for both the mechanism with and without backlash. The effect of roller diameter d_r is clear from expression (43), where roller diameter d_r is in the denominator.
2. The occurrence of backlash $\Delta_j(\beta)$ in the mechanism admittedly reduces losses P_C due to the smaller number of rollers involved in the transmission of load torque M_K , but it also reduces the precision of operation, as can be seen by comparing the values of angles β_k^m presented in Tables 2 and 3.
3. Reducing the number n of rollers and increasing their diameter d_r also negatively affects the precision of the work, but not to the same extent as due to backlash $\Delta_j(\beta)$. This is clear from comparing the values of the angle β_k^m for cases 1 and 2 with each other in Tables 2 and 3.
4. Although decreasing the number n of rollers and increasing their diameter d_r results in an increase in loads $F_j(\beta)$, as shown in Figures 11a and 13a, it has a beneficial effect on the contact pressure $p_j(\beta)$ as it reduces their value (Figures 11b and 13b).
5. The mechanical power losses P_C in the discussed output mechanism will be lower if it is used in a cycloidal gearbox with a small value of eccentricity e . However, the choice of eccentricity e should ultimately be considered in terms of cycloidal gearing. This follows from expression (43), where eccentricity e is in the numerator.
6. Analyzing the model of mechanical power losses P_C (43) in terms of the impact of ratio u of the cycloidal gearbox, it can be concluded that as ratio u increases, its impact on losses P_C decreases. With an increase in the value of the ratio u , the partial expression $(u + 1/u)$ of equation (43) tends to 1. Thus, using the discussed output mechanism in gearboxes with ratio $u > 30$ is preferable.

Author Contributions: Conceptualization, S.B.; methodology, P.A., S.B.; investigation, S.B.; writing—original draft preparation, P.A., S.B.; writing—review and editing, S.B.; visualization, S.B.; supervision, S.B. All authors have read and agreed to the published version of the manuscript.

Funding: This research received no external funding.

Data Availability Statement: Data are available on request.

Conflicts of Interest: The authors declare no conflicts of interest.

References

1. Malhotra, S.K.; Parameswaran, M.A. Analysis of a cycloid speed reducer. *Mech. Mach. Theory* **1983**, *18*, 491–499. [[CrossRef](#)]
2. Davoli, P.; Gorla, C.; Rosa, F.; Longoni, C.; Chiozzi, F.; Samarani, A. Theoretical and experimental analysis of a cycloidal speed reducer. *J. Mech. Des.* **2008**, *130*, 112604-1–112604-8.
3. Mačkić, T.; Babić, Ž.; Kostić, N.; Blagojević, M. Cyclo drive efficiency. In Proceedings of the 13th International Conference on Tribology—Serbiatrib'13, Kragujevac, Serbia, 15–17 May 2013; pp. 230–233.
4. Matejić, M.; Blagojević, M.; Cofaru, I.I.; Kostić, N.; Petrović, N.; Marjanović, N. Determining efficiency of cycloid reducers using different calculation methods. In Proceedings of the 9th International Conference on Manufacturing Science and Education—MSE, Sibiu, Romania, 5 June 2019; pp. 1–7.
5. Blagojevic, M.; Kocic, M.; Marjanovic, N.; Stojanovic, B.; Dordevic, Z.; Ivanovic, L.; Marjanovic, V. Influence of the friction on the cycloidal speed reducer efficiency. *J. Balk. Tribol. Assoc.* **2012**, *18*, 217–227.
6. He, W.; Lu, Q. Transmission efficiency analysis of pin-cycloid planetary gearing reducer applying two-stage speed reduction used in propeller pitch variator. *Adv. Mater. Res.* **2011**, *199–200*, 409–415. [[CrossRef](#)]
7. Olejarczyk, K.; Wikło, M.; Kołodziejczyk, K.; Król, K.; Nowak, R. Experimental impact studies of the application mineral oil and synthetic oil on the efficiency of the single-gear cycloidal. *Tribologia* **2017**, *1*, 67–73. [[CrossRef](#)]
8. Blanche, J.G.; Yang, D.C.H. Cycloid drives with machining tolerances. *ASME J. Mech. Des.* **1989**, *111*, 337–344. [[CrossRef](#)]
9. Pham, A.D.; Ahn, H.J. Efficiency analysis of a cycloid reducer considering tolerance. *J. Frict. Wear* **2017**, *38*, 490–496. [[CrossRef](#)]
10. Bednarczyk, S.; Jankowski, L.; Krawczyk, J. The influence of eccentricity changes on power losses in cycloidal gearing. *Tribologia* **2019**, *3*, 19–29. [[CrossRef](#)]
11. Lin, K.-S.; Chan, K.-Y.; Lee, J.-J. Kinematic error analysis and tolerance allocation of cycloidal gear reducers. *Mech. Mach. Theory* **2018**, *124*, 73–91. [[CrossRef](#)]

12. Li, X. A dynamic model to predict the number of pins to transmit load in a cycloidal reducer with assembling clearance. *Proc. Inst. Mech. Eng. Part C J. Mech. Eng. Sci.* **2019**, *233*, 4247–4263.
13. Bednarczyk, S. Analysis of the cycloidal reducer output mechanism while taking into account machining deviations. *Proc. Inst. Mech. Eng. Part C J. Mech. Eng. Sci.* **2021**, *235*, 7299–7313. [[CrossRef](#)]
14. Blagojevic, M.; Marjanovic, N.; Djordjevic, Z.; Stojanovic, B.; Disic, A. A new design of a two-stage cycloidal speed reducer. *J. Mech. Des.* **2011**, *133*, 085001-1–085001-7. [[CrossRef](#)]
15. Bednarczyk, S.; Kalita, M. Reduktor Dwustopniowy Cykloidalny. Patent PL 241110 B1, 1 August 2022.
16. Maccioni, L.; Concli, F.; Blagojevic, M. A new three-stage gearbox concept for high reduction ratios: Use of a nested-cycloidal architecture to increase the power density. *Mech. Mach. Theory* **2023**, *181*, 105203. [[CrossRef](#)]
17. Xu, L.X.; Zhong, J.L.; Li, Y.; Chang, L. Design and dynamic transmission error analysis of a new type of cycloidal-pin reducer with a rotatable output-pin mechanism. *Mech. Mach. Theory* **2023**, *181*, 105218. [[CrossRef](#)]
18. Huang, J.; Li, C.; Chen, B. Optimization design of RV reducer crankshaft bearing. *Appl. Sci.* **2020**, *10*, 6520. [[CrossRef](#)]
19. Lei, S.; Shunke, L.; Weihua, L.; Feixin, C. Comparison of the key structures between RV reducer and Spinea reducer based on finite element method. In *Application of Intelligent Systems in Multi-Modal Information Analytics*; Sugumaran, V., Xu, Z., Shankar, P., Zhou, H., Eds.; MMIA 2019. Advances in Intelligent Systems and Computing, 929; Springer: Cham, Switzerland, 2019. [[CrossRef](#)]
20. Fiorineschi, L.; Frillici, F.S.; Pugi, L.; Federico Rotini, F. Impact of Cycloid's and Roller's Dimensional Errors on the Performance of a Cycloidal Drive for Power Transmission. *Machines* **2023**, *11*, 772. [[CrossRef](#)]
21. Sun, X.X.; Liang, H. A new numerical force analysis method of CBR reducer with tooth modification. *J. Phys. Conf. Ser.* **2019**, *1187*, 032053. [[CrossRef](#)]
22. Sun, X.X.; Han, L.; Ma, K.; Li, L.; Wang, J. Lost motion analysis of CBR reducer. *Mech. Mach. Theory* **2018**, *120*, 89–106. [[CrossRef](#)]
23. Hsieh, C.-F. The effect on dynamics of using a new transmission design for eccentric speed reducers. *Mech. Mach. Theory* **2014**, *80*, 1–16. [[CrossRef](#)]
24. Tran, T.L.; Pham, A.D.; Cho Ch Ahn, H.J. Torsional rigidity analysis of cycloid reducers considering tolerances. In Proceedings of the 16th Asia Pacific Vibration Conference, 2015 HUST, Hanoi, Vietnam, 24–26 November 2015; pp. 1–6.
25. Popov, V.L. Contact Mechanics and Friction. In *Physical Principles and Applications*; Springer: Berlin/Heidelberg, Germany, 2010; p. 63.
26. Contact Stresses and Deformations, ME EN 7960-Precision Machine Design Topic 7. Available online: <http://www.mech.utah.edu/~me7960/lectures/Topic7-ContactStressesAndDeformations.pdf> (accessed on 12 May 2024).
27. Pytko, S. Problemy tarcia tocznego. In *Wybrane Problemy Tribologii*; PWN: Warszawa, Poland, 1990; pp. 47–67.

Disclaimer/Publisher's Note: The statements, opinions and data contained in all publications are solely those of the individual author(s) and contributor(s) and not of MDPI and/or the editor(s). MDPI and/or the editor(s) disclaim responsibility for any injury to people or property resulting from any ideas, methods, instructions or products referred to in the content.